

# Model Simulations of Local Meteorological Conditions in the Vicinity of a Hypothetical Nuclear Power Plant in Jordan

Marwan M. Al-Kloub<sup>1,2</sup>, Alexander Mahura<sup>3</sup>, Alexander Baklanov<sup>4,5</sup>, Nahid Atashi<sup>3,6</sup>, Tareq Hussein<sup>1,3</sup>\*

<sup>1</sup>The University of Jordan, School of Science, Department of Physics, Jordan

<sup>2</sup>Prince Faisal Technical College, Department of Physics, Jordan

<sup>3</sup>University of Helsinki (UHES), Faculty of Science, Institute for Atmospheric and Earth System Research (INAR/Physics), Finland

<sup>4</sup>World Meteorological Organization (WMO), Switzerland

<sup>5</sup>University of Copenhagen (UCPH), Niels Bohr Institute (NBI), Denmark

<sup>6</sup>University of Isfahn, Faculty of Geographical science and Planning, Iran

Received 22 June 2019, Accepted 6 October 2019

## Abstract

As a solution for the increasing energy demand in Jordan, nuclear power was recommended for the energy mix at the national level. However, investigations of the meteorological conditions and mass transfer have never been conducted and reported earlier based on typical Jordanian conditions in order to have prior knowledge in case of a future hypothetical nuclear accident in Jordan. In this study, the variabilities of horizontal and vertical wind components and surface temperature differences have been investigated near one of the originally suggested locations for the construction of a nuclear power plant facility. That proposed location is the site of the Samra Energy Power Plant (SEPP). The selected domain of the simulation model was 85×85 km<sup>2</sup> in area (17×17 grid points and 13 vertical layers) surrounding the SEPP site. The simulations revealed that the wind direction near the surface was developed to comply with the complexity of the terrain regardless of the input values of the prevailing wind direction. The wind direction propagated along the valleys that are surrounded by the dominating mountains. The surface wind speed was proportional to the input value of the wind speed as well as to the slope of the surrounding terrain. Quantitatively, the developed surface wind speed was 0.5–2.1 m/s in January compared with 1.0–4.3 m/s in July. The vertical component of wind velocity was the lowest (nearly zero in January versus ~0.1 m/s in July) near the surface. In practice, the main outcome of this investigation can serve as a base-block for considering other possible geographical locations for the construction of a nuclear power plant in Jordan and for case studies intended to assess possible consequences in case of accidental releases and other potential accidents of possible nuclear, chemical, industrial danger.

© 2020 Jordan Journal of Earth and Environmental Sciences. All rights reserved

**Keywords:** meteorological modeling, nuclear power plant, horizontal and vertical components of wind speed, surface temperature difference

## 1. Introduction

In general, it is difficult and rather complex to make a correct and clear decision in a dangerous situation, especially at the initial stages, based on the availability of exhaustive information that might be delayed to reach the hands of decision-makers. Therefore, it is wise to make preliminary estimations on the basis of information prepared beforehand regarding a hypothetical nuclear accident and its possible consequences. On the whole, nuclear power plant (NPP) accidents involve emissions of radioactive pollutants into the environment and their transport in the atmosphere covering large geographical regions. Although nuclear safety at NPPs is very strict and tight that accidents are less probable to happen; however, such events were recorded several times in the past. According to the International Nuclear Event Scale (INES; levels 1-7), two accidents of the highest level (7) were reported in the past, namely Chernobyl, Ukraine in 1986 and Fukushima Daiichi, Japan in 2011.

For the purpose of securing prior knowledge for the sake of making a clear decision during nuclear accidents, mathematical models can be utilized to simulate the physical

and dynamical processes of radionuclides' atmospheric transport, dispersion, removal, and deposition (e.g. Cao et al., 20016; Mitrakos et al., 2016; Lauritzen et al., 2007; Baklanov, 2003; Mahura et al., 1999; Baklanov et al., 1994). This can help understand and forecast the transport of radioactive emissions from potential sources that play a considerable role in the preparation of valuable data for decision-making processes. From a large diversity of factors, influenced by the environmental consequences of accident situations, the considerable part of the preparation of data is more influenced by local peculiarities and regional conditions. These conditions include: location of accident source, geographic peculiarities of local terrains; climatic conditions; density and quantity of the population; character and types of urban settlements, etc. As a matter of fact, creating centers for ecological monitoring and forecasting accidental consequences are especially important at both the local and regional levels.

After being emitted into the atmosphere, radioactive pollution clouds undergo additional changes such as: advection, turbulence, radioactive decay, dry and wet

\* Corresponding author e-mail: t.hussein@ju.edu.jo

deposition, etc. (e.g. Matsuda et al., 2017; Evangelidou et al., 2016; Mészáros et al., 2012; Momoshima and Bondietti, 1994). Many models, describing the distribution of radioactive emissions from NPPs, have been developed and applied worldwide (e.g. Christoudias et al., 2014; Kawamura et al., 2014; Mazur et al., 2014; Baklanov et al., 2008a and 2008b; Mahura et al., 2005; Srinivas and Venkatesan, 2005; Baklanov and Mahura, 2001; Glyshenko et al., 1981; Davydova et al., 1990; AGROS). The Gaussian models require a minimum of input data; and hence, these are simple to simulate the distribution and transport of emissions. However, such models are not fully realistic, because they assume a homogeneous vertical distribution of pollution, whereas, in reality, the normal distribution law does not always occur. Besides, the wind velocity measurement is usually sparse and sometimes the trajectory of radioactive cloud is represented by a straight line. This limits the application of this model to an approximate distance between 10 and 15 km. Therefore, a more detailed description of emissions' distribution from NPP requires the application of higher order models, through which it is necessary to take into account temporal and spatial wind velocity components' changes. Such models require information about the velocity at several points (e.g. observation stations). The complex three-dimensional (3D) models, which are based on 3D wind fields, are capable of taking into account the influence of the surrounding terrain, roughness of the surface, wind change, atmospheric stability, etc. Such models are also embedded with the Atmospheric Boundary Layer (ABL) models in order to have better simulation results for the vertical and spatial structure of the wind field and turbulence. Typically, the effective source height of pollution, the increase of initial concentration at different stages of the accidental release, changes in concentration due to processes of the radioactive decay, wet and dry deposition removal of radionuclides from the atmosphere are also taken into account under the simulation of the distribution of emissions.

In 2001, Jordan started working on its own national nuclear power programme by establishing the Jordan Nuclear Energy Commission (JNEC). In 2007, the JNEC was replaced by the Jordan Nuclear Regulatory Commission (JNRC), and in 2008, it was replaced by the Jordan Atomic Energy Commission (JAEC). The JNRC works in coordination with relevant organizations to regulate and monitor nuclear energy, to protect the environment from radioactive hazards and related pollution, and to ensure the requirements for radiation safety, protection, and security. The JNRC also works closely with the International Atomic Energy Agency (IAEA) to apply nuclear safety standards in Jordan. The main objective of the JAEC has been to promote and develop a peaceful utilization of atomic energy to produce electricity and desalinate water.

The Jordanian nuclear programme also includes a research nuclear power plant, which has been established on the campus of the Jordan University of Science and Technology with a capacity of 5-10 MWatt (MW). The main purpose of this research plant is to conduct scientific research in medical, agricultural, and health sciences and services. Jordan also accommodates the International Centre for

Synchrotron-Light for Experimental Science Applications in the Middle East (SESAME), which is ought to be the first major international research center in the Middle East with collaboration between the JAEC and the United Nations Educational, Scientific and Cultural Organization (UNESCO).

Originally, Jordan aimed to have two 1000 MW water-water energetic reactor units (VVER-1000) in operation by 2025, but is now reconsidering the use of smaller modular reactors instead. The exact locations of NPP's units have been under continuous consideration and analysis. One of originally suggested locations was near the Samra Electric Power Plant (SEPP) located in the northeastern part of Jordan.

The main objectives of this study are to simulate and investigate the meteorological conditions over the domain (85×85 km<sup>2</sup>) centering around the SEPP site. It should be noted that this kind of investigation regarding the Jordanian conditions has never been made or published before. In practice, the study presented in this manuscript may serve as a base-block to consider other possible geographical locations in Jordan and to conduct case studies for the assessment of other potential objects that pose possible nuclear, chemical, and industrial threats.

## 2. Three-dimensional meso-meteorological model

### 2.1 Model description

This study utilizes a modified version of the Model Package (MP) named after the Institute of the Northern Environmental Problems (INEP), developed for the Simulation of Meteorological Fields (METEO) and Distribution of Pollution within the Atmospheric Boundary Layer (TRANS). This MP includes a three-dimensional (3D) modeling system that describes atmospheric dynamics and radioactive pollution within a modeling domain near a nuclear power plant. It consists of two main parts (e.g. Baklanov et al., 1994) as follows:

- (1) METEO: a numerical meso-meteorological model over a complex terrain around a nuclear power plant to simulate the 3D meteorological fields
- (2) TRANS: an Eulerian transport model to simulate the 3D atmospheric transport, diffusion, and deposition of a variety of radioactive pollutants over the terrain due to a hypothetical accident at the selected nuclear power plant as well as to calculate doses due to inhalation from the passing radioactive clouds and from the surfaces of different human organs of different population groups.

The MP was developed by a team of the researchers from INEP of the Kola Science Center, Russian Academy of Science. It was utilized for various case-studies (e.g. Baklanov et al., 1994; Baklanov et al., 2000; Baklanov et al., 2002). In this particular study, the MP was modified and prepared to accommodate for the typical Jordanian conditions of the complex terrain and to simulate the meteorological fields within the boundaries of the selected domain (within a 85×85 km<sup>2</sup> zone around a hypothetical NPP in the northeastern part of Jordan). This paper is focused on running the first part of the MP package (METEO - i.e. the meteorological fields' simulation). Although the MP second part (TRANS - i.e. distribution and atmospheric transport

of radioactive pollution and calculation of doses) is also of great interest in this regard, it will be presented in details in another paper in the nearest future.

The METEO model can be extended from a very local scale to larger scales. The concept of the 3D wind field is typically used in the most complex 3D models, so it is possible to take into account the influence of the terrain, roughness, wind characteristics, atmospheric stability, and other factors.

The numerical simulation of atmospheric pollution transport processes and diffusion consists of model realizations of pollution distribution (e.g. TRANS) based on the determination of both the  $u,v,w$  - components of wind field  $U$ , and coefficients of turbulent diffusion  $K$  along  $x,y,z$ -directions. The wind fields can be determined by a combined objective analysis of meteorological data obtained from a meteorological measurement network and mathematical modeling of the hydrothermodynamical characteristics of the atmospheric boundary layer. Even without an existing meteorological measurement network, the fields can be determined by means of modeling only. However, validation is still required against ground-based measurements. The details of the TRANS model description are explained by e.g. Baklanov et al. (1994).

The main components of the METEO-part are: (1) equations to describe the atmospheric processes, (2) a system of equations to describe the atmospheric surface layer in small-angle cases of a terrain, (3) boundary and initial conditions, and (4) determination of surface temperature by using actual measurements or by utilizing radiation and the heat balance equation of an orographic non-homogeneous surface. The use of special methods in the solution of model equations, including the system of coordinates with reducing height and the method of fictitious domains, allows for the simulation of the dynamics of the atmosphere over an arbitrary terrain.

### 2.2 Model input and output

The METEO model requires a set of input variables (see Tables 1–3). These include parameters related to the terrain and its contents (location of the nuclear power plant (thereafter, the plant) and water surfaces in the selected model domain), characteristics and operation mode of the plant, temporal parameters related to the occurrence of a hypothetical accident, a series of meteorological parameters and numerical parameters. The output of the METEO simulations includes 3D arrays that describe (in  $y$ -latitude,  $x$ -longitude, and  $z$ -altitude directions) the wind and turbulence fields as well as the temperature difference within the terrain at selected time-steps after the occurrence of a hypothetical accident.

The terrain parameters consist of a relief for the local terrain in the selected model domain, which is a 2D array that contains the height of a point above the sea level (a.s.l.). This digital map is scaled down or up when it is needed, so that the vertical structure of the model covers most of the boundary layer above the terrain. Other terrain-related parameters are locations and altitudes of water surfaces and the plant in the domain. The temporal parameters of the accident include time (hour and minute) and date (year, month, and day) of the

accident's starting time. The numerical parameters include: a 3D grid description (number of grid points in the three  $x$ ,  $y$ ,  $z$ -directions), simulation time-step [s], continuity of time-step [s], number of steps and duration of step for iteration procedures, and a number of steps and intervals at which to write/save the results to the output files.

The meteorological parameters describe the conditions within the terrain at the location of the source (i.e. the plant). These include: wind direction and speed [in degrees from north and  $m\ s^{-1}$ , respectively], ambient air temperature [ $^{\circ}C$ ], relative humidity [in %], intensity and quantity of precipitation [in  $mm/h$  and  $mm$ ]. Such parameters are additionally required to be collected (of course, if available for as many locations as possible from a nearby meteorological network of measurements). Other meteorological background variables include: air temperature gradient [ $^{\circ}C$ ], Coriolis parameters [ $s^{-1}$ ], buoyancy parameters, 3D coefficient of turbulence, lambda constant, air density [ $kg\ m^{-3}$ ], vertical wind profile description, surface temperature initial condition, as well as the temperature difference between land surface and air, between water surface and air, and between "hot" water surface (e.g. water used for cooling NPP and released into a nearby water object) and air.

### 3. Case studies

In this study, a series of the METEO model simulations have been performed for the location of the hypothetical NPP (which coincides with the SEPP location as one of previously and originally suggested locations to construct the Jordanian NPP) and its surrounding domain (Figure 1). The METEO model simulations were performed on a monthly basis taking into account the dominating average meteorological conditions (based on a statistical analysis of the available climatological data; see Table 3).

#### 3.1 Site location and surrounding terrain

Although the exact location of the planned NPP in Jordan has not been certain yet, the model simulations have been made to investigate the Jordanian conditions and extend this exercise to other suggested locations in the future. The Samra EPP is located in the northeastern part of Jordan ( $32.1443^{\circ}N$ ,  $36.1428^{\circ}E$ ) at an altitude of  $\sim 560$  m (see Figure 1c). It is about 30 km to the north-east of Amman (the Jordanian capital city) and about 10 km to the north-east of Zarqa (Figure 1b). These two cities accommodate most of the Jordanian population (that is  $\sim 10$  million inhabitants, [www.worldmeters.info](http://www.worldmeters.info), 2019).

For this study, a model domain (size of  $85 \times 85\ km^2$ ) has been selected and at the center of which the NPP plant is placed (Figure 1d). It should be noted that the original terrain topography (Figure 1c) is very complex with about  $\sim 110$  m a.s.l. at the south-west (near the Jordan Valley) and three mountains to north-west, south-west, and north-east with heights of about  $\sim 1240$  m,  $\sim 1050$  m, and  $\sim 1100$  m, respectively. The terrain has a valley along the east-west line between the aforementioned mountains. This valley divides the terrain into rather equal halves, and it is nearly 10 km wide at the eastern side (height  $\sim 550$  m) of the terrain, but becomes very narrow (less than 4 km wide) and deeper (down to heights of even  $\sim 10$  m) at the western side of the domain. There are also small-size water reserves, which are located close to the power plant.

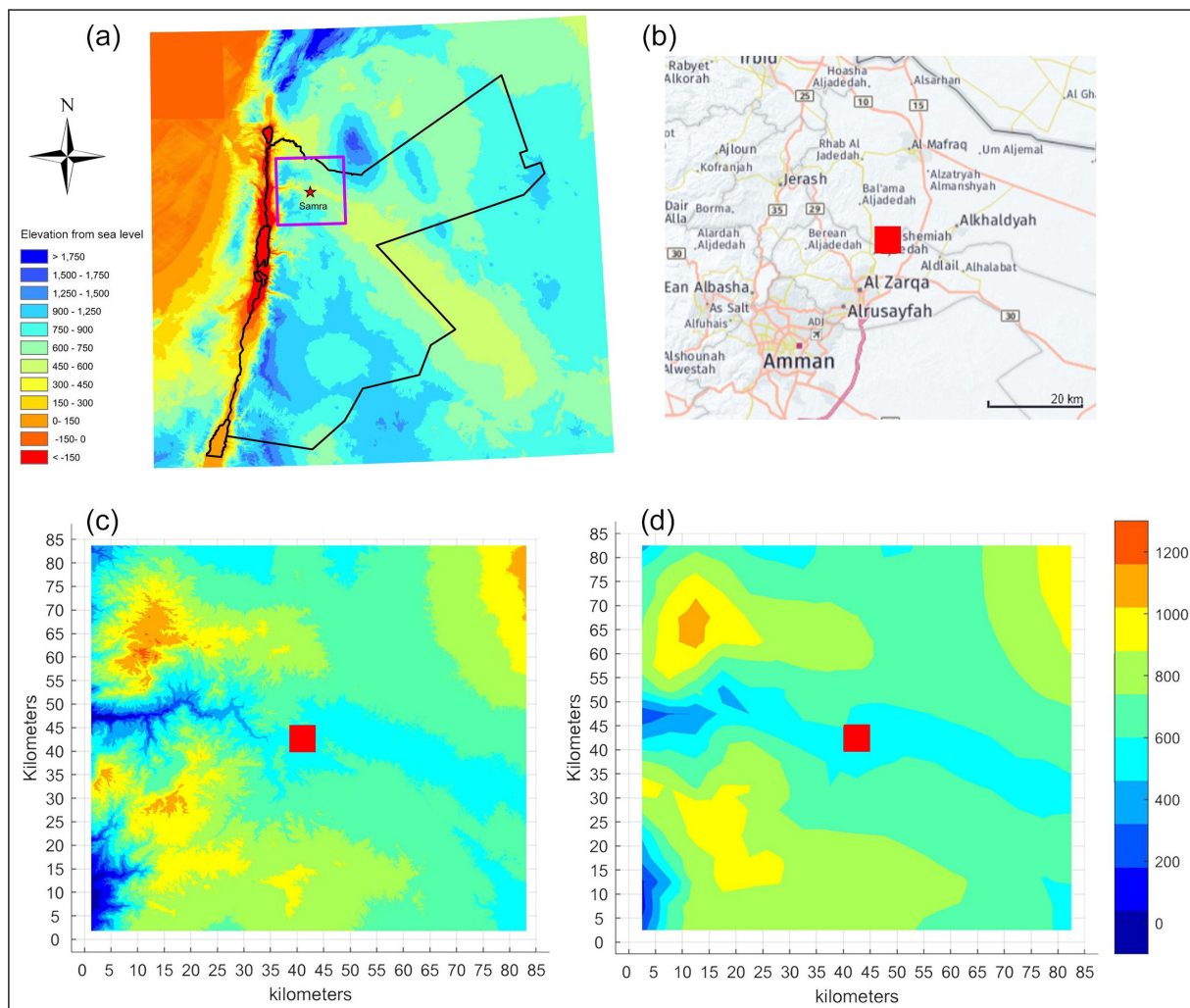


**Figure 1.** (a) Jordan map showing elevation above sea level and the domain (red square corresponding to  $85 \times 85 \text{ km}^2$ ), which is also shown from three different perspective: (b) land use, (c) detailed map of elevation above sea level, and (d) converted elevation map as  $17 \times 17$  grid. The location of the hypothetical Jordanian nuclear power plant (hJNPP) is marked by a red square in the middle of the domain.

The original digital map of the terrain (Figure 1c) was transformed by interpolating into a  $17 \times 17$  grid domain with a 5000 m horizontal resolution (Figure 1d). It was used as an input pre-defined terrain data for the METEO model simulations. The power plant and the nearby water surfaces lied within the same grid cell, which was located at  $\sim 560 \text{ m a. s. l.}$  For practical purposes, the whole pre-defined terrain was “lowered down” by 200 meters, and hence, the original heights of locations of NPP and water surfaces were shifted down to 358 m in the model domain. This was done in order to accommodate more vertical levels in the atmosphere for better representation of hypothetical emissions by vertical layers. In total, there are thirteen vertical levels covering a 1300 m depth layer. Here, the depth of each sub-layer is as follows: 50 m – for 1-5<sup>th</sup> layers, 75 m – 6<sup>th</sup>, 100 m – 7<sup>th</sup>, 125 m – 8<sup>th</sup>, 150 m – 9-13<sup>th</sup> layers. Table 1 lists the details of the inputs related to the terrain, domain, and model simulation parameters.

### 3.2 Meteorological conditions

The meteorological parameters which are required as inputs for the METEO model simulation are listed in Table 2. The main meteorological parameters (wind speed and direction, ambient air temperature, relative humidity, and hourly and daily precipitation) were obtained from continuous measurements at

the selected weather station. The year 2017 was considered as the most typical year in a series of observations starting with 2015 at the campus of the University of Jordan ( $32.0160^\circ \text{N}$ ,  $35.8695^\circ \text{E}$ ). The statistics of monthly (from January until December) variabilities of these meteorological parameters are summarized in Table 3 (Hussein et al., 2018). The monthly mean ambient air temperature varied between  $+7$  and  $+26.5^\circ \text{C}$  (the coldest in January and the warmest in July). The monthly mean relative humidity was inversely proportional to the temperature, and it was within the range of 38–78% (the highest in January and the lowest in July). The wettest month was February (daily mean precipitation of 5.52 mm/day; with the highest hourly rainfall being 0.23 mm/h and the driest months being May-June-July and September with no precipitation observed). Based on the monthly analysis of the wind characteristics, the prevailing wind direction varied from SE ( $\sim 145^\circ$ , November) to NW ( $\sim 321^\circ$ , September). In particular, the winds from the north-western sector dominated over the period from April to October, the winds from the south-eastern sector prevailed from November to December, and winds from the south-western sector dominated from January to March. The magnitude of the wind speed was in the range of 1–1.9 m/s (the highest in July and the lowest in October). Lower wind speeds were observed during the period from October to December, and the period for higher wind speeds was from June to August.

**Table 1.** Geographical properties of the model simulation and their numerical input parameters

|           | Parameter   | Note                                       | Assigned value   |
|-----------|---|--|--|
| Terrain   | Relief for local terrain  | XY grid points                             | 85×85 km <sup>2</sup> on a 17×17 grid<br>Figure 2  |
|           | Relief grid resolution  | arbitrary                                  | 5000 meters for 85×85 km <sup>2</sup>  |
|           | Geographical locations of:<br>- nuclear power plant<br>- water surfaces | assigned to a certain cell in the terrain  | nuclear power plant at the middle of the terrain<br>(i.e. cell (9,9))<br>water surfaces were assigned to closest cells       |
|           | Altitude of:<br>- nuclear power plant<br>- water surfaces               | assigned after scaling up/down the terrain | on the downward scaled (85×85 km <sup>2</sup> ) domain,<br>nuclear power plant at 358 m and water surfaces<br>358 m          |
| Numerical | 3D grid-points  | arbitrary                                  | 17×17 (85×85 km <sup>2</sup> ); Figure 2   |
|           | Simulation time   | arbitrary                                  | 180 minutes  |
|           | Continuity of time step   | arbitrary                                  | 60 s   |
|           | XY grid steps   | identical for X and Y                      | 5000 m for 85×85 km <sup>2</sup>   |
|           | Vertical profile  | 13 layers                                  | 1300 meters vertical profile:<br>layers 1-5: 50 m<br>layer 6: 75 m<br>layer 7: 100 m<br>layer 8: 125 m<br>layers 9-13: 150 m |
|           | Time step iteration   | arbitrary                                  | 10 seconds   |
|           | Output steps  | arbitrary                                  | every 10 minutes   |

**Table 2.** Model input that describe the meteorological conditions.

|                | Parameter                  | Note  | Assigned value  |  |
|----------------|----------------------------|---|---|--|
| Meteorological | Wind direction             | North à 0° (clock-wise)   | Table 3   |  |
|                | Wind speed                 | $WS = \sqrt{U^2 + V^2}$<br><i>U</i> and <i>V</i> are horizontal components  | Table 3   |  |
|                | Ambient temperature        | Measured at 2 meters  | Table 3   |  |
|                | Relative humidity          | Measured at 2 meters  | Table 3   |  |
|                | Intensity of precipitation | Measured  | Table 3   |  |
|                | Quantity of precipitation  | Measured  | Table 3   |  |
|                | Temperature gradient       | Temperature vertical gradient (dry vs humid atmosphere)   | dry adiabatic condition (0.01 °C/m)   |  |
|                | Coriolis parameters        | $f = 2\Omega \sin\phi$<br>$\phi$ is the latitude<br>$\Omega = 2\pi/T$ is the Earth's rotation rate<br>(7.2921×10 <sup>-5</sup> rad/s and <i>T</i> = 23 hr 56 m 4.1 s) | For the altitude at Samra Electric Power Plant<br>$f = 7.71 \times 10^{-5} \text{ s}^{-1}$  |  |
|                | Buoyancy parameter         | 0.003 – 0.01  | 0.003   |  |
|                | 3D turbulence coefficient  | Coefficients of turbulent diffusion assigned depending on horizontal vs vertical resolution   | XY plane (5000) and Z direction (50)  |  |
|                | Lambda constant            | Constant for turbulence modeling to calculate fluxes  | 0.035   |  |
|                | Air density                | ideal gas law   | 1.18 kg/m <sup>3</sup>  |  |
|                |                            | Vertical wind profile   | 1- Linearly increasing with height within first 4 layers of the domain (up to 200 m). Above that, a steady-state profile is assumed<br>2- Exponentially increasing with height within the first 8 levels (up to 550m). Above that, a steady-state profile is assumed<br>3- Exponentially increasing with height within the first 4 levels (up to 200m). Above that, a steady-state profile is assumed | We selected the second option            |
|                |                            | Surface temperature initial condition   | 1- $PSI(i,j) = 0$ whole domain<br>2- Assumes temperature difference:<br>land surface and air ( $T_{land} - T_a$ )<br>water surf and air ( $T_{water} - T_a$ )<br>hot-water and air ( $T_{hot-water} - T_a$ )  | We selected the second option<br>Table 3 |

The model simulation also requires the temperature difference between the land surface and air ( $T_l - T_a$ ), water surface and air ( $T_w - T_a$ ), and “hot” water and air ( $T_{hw} - T_a$ ). These were adopted from the “World Climate Guide” and are listed in Table 3. The  $T_l - T_a$  was in the range of 1–4°C (the highest in August and the lowest during December–March). The  $T_w - T_a$  varied from +3°C to -2°C (the highest was in December-January, whereas the lowest (and negative) was during May–July), and it was negative during April–September. The  $T_{hw} - T_a$  difference followed a rather similar monthly trend as that of the  $T_w - T_a$  difference but it was

always positive and had a range of 1–6 °C (the highest was in December-January whereas the lowest was during May–July).

### 3.3 Model simulations

As mentioned before, the meteorological field simulations were performed based on monthly mean inputs, which are listed in Table 3. The main obtained results for the horizontal wind speed are presented in Figures 2–4, vertical mixing in Figure 5, and surface temperature difference is presented in Figure 6 summarized for winter (January), and summer (July), and averaged over all the twelve months.

**Table 3.** Monthly means of the weather conditions and temperature differences [°C] between land surface and air ( $T_l - T_a$ ), water surf and air ( $T_w - T_a$ ), and hot-water and air ( $T_{hw} - T_a$ ). The weather data was obtained from the measurement at the campus of the University of Jordan during 2017. The data for temperature differences was obtained from the “World Climate Guide”.

| Month | Temp. [°C] | RH [%] | Wind Speed [m/s] | Wind Direct. [degree] | Hourly Rainfall [mm/h] | Daily Rainfall [mm] | $T_l - T_a$ | $T_w - T_a$ | $T_{hw} - T_a$ |
|-------|------------|--------|------------------|-----------------------|------------------------|---------------------|-------------|-------------|----------------|
| Jan   | 7.0        | 78     | 1.4              | 232                   | 0.14                   | 3.36                | 1.0         | 3.0         | 6.0            |
| Feb   | 8.7        | 63     | 1.6              | 226                   | 0.23                   | 5.52                | 1.0         | 2.0         | 5.0            |
| Mar   | 12.9       | 62     | 1.5              | 265                   | 0.03                   | 0.72                | 1.0         | 1.0         | 4.0            |
| Apr   | 17.1       | 49     | 1.4              | 284                   | 0.03                   | 0.72                | 2.0         | - 1.5       | 1.5            |
| May   | 20.8       | 42     | 1.6              | 291                   | 0.00                   | 0.00                | 2.0         | - 2.0       | 1.0            |
| Jun   | 23.9       | 49     | 1.8              | 304                   | 0.00                   | 0.00                | 2.0         | - 2.0       | 1.0            |
| Jul   | 26.5       | 38     | 1.9              | 313                   | 0.00                   | 0.00                | 3.0         | - 2.0       | 1.0            |
| Aug   | 26.3       | 52     | 1.8              | 312                   | 0.02                   | 0.48                | 4.0         | - 1.0       | 2.0            |
| Sep   | 24.7       | 52     | 1.4              | 321                   | 0.00                   | 0.00                | 3.0         | - 1.5       | 1.5            |
| Oct   | 21.1       | 56     | 1.0              | 308                   | 0.17                   | 4.08                | 2.0         | 1.0         | 4.0            |
| Nov   | 14.3       | 68     | 1.1              | 145                   | 0.04                   | 0.96                | 2.0         | 2.0         | 5.0            |
| Dec   | 8.1        | 76     | 1.1              | 188                   | 0.14                   | 3.36                | 1.0         | 3.0         | 6.0            |

*Comment: the temperature differences are calculated based on data from the World Climate Guide website (<https://www.climatestotravel.com/climate/jordan> - publicly accessible) containing also averaged climatological data for air, sea/water temperatures.*

The horizontal wind speed profiles are presented for model layer 8 (425–550 m), layer 10 (700–850 m), and layer 12 (1000–1150 m) after 60, 120, and 180 minutes (Figures 2–4) of model simulations. In general, the wind characteristics (speed and direction) were originally developed near the surface to comply with the complexity of the terrain surrounding the studied site. They, then, further propagated along the valleys that are surrounded by dominating mountains. Although the input values of the prevailing wind direction for the model simulations (see Table 3) were different between January and July, the wind direction near the surface was almost similar for all months; i.e. drifting parallel to the valleys (Figure 2a–f, Figure 3a–f, and Figure 4a–f). At the top layer of the model domain, the wind direction and speed were aligned with the monthly input values (i.e. magnitudes of wind speed and prevailing wind direction). As for the wind speed near the surface, it

was higher in July than in January (i.e. proportional to the input value). Furthermore, the wind speed was proportional to the slope of the terrain. Quantitatively, after 180 minutes of simulations, the wind speed near the NPP location and close to the terrain surface was in the range 1.3–2.0 m/s in January (Figure 4a) and was slightly higher (1.4–2.6 m/s) in July (Figure 4d). The annual mean wind speed was 1–2 m/s (Figure 4g). Along the valley towards the west sector, the surface wind speed was in the range of 0.5–2.1 m/s in January and 1.0–4.3 m/s in July (annual mean 0.5–3.4 m/s) with the prevailing wind direction down the valley being towards the west. Along the valley towards the east, the surface wind speed was in the range of 1.4–2.1 m/s in January and 2.9–3.2 m/s in July (annual mean 0.7–2.3 m/s) with the prevailing wind direction along the valley being towards the east. The valley on the west side of the domain was steeper and narrower than the valley on the east side.

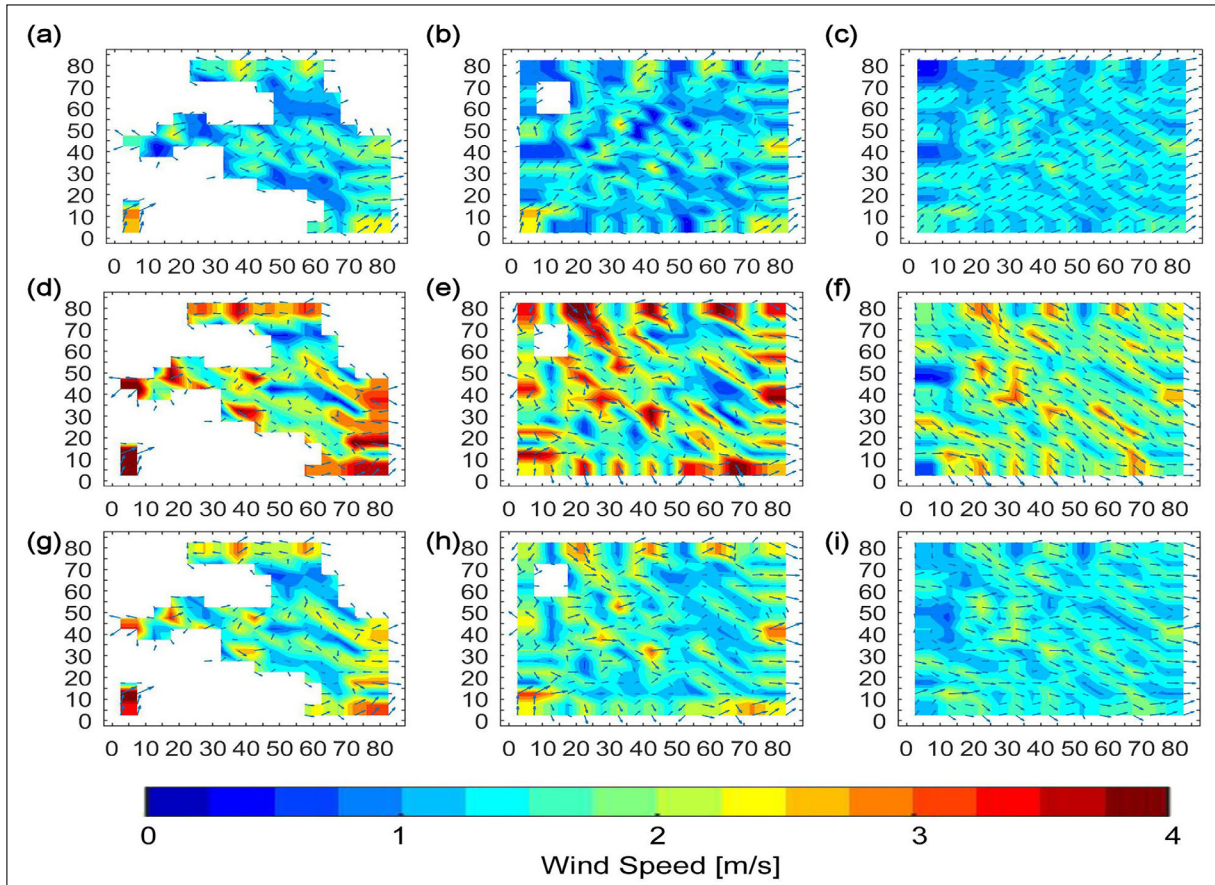


**Figure 2.** Wind fields simulation after 60 minutes for (a–c) January, (d–f) July, and (g–i) overall annual average. Each row subplots respectively show the simulation results for the model layer 8 (425–550 m.a.s.l.), layer 10 (700–850 m.a.s.l.), and layer 12 (1000–1150 m.a.s.l.).

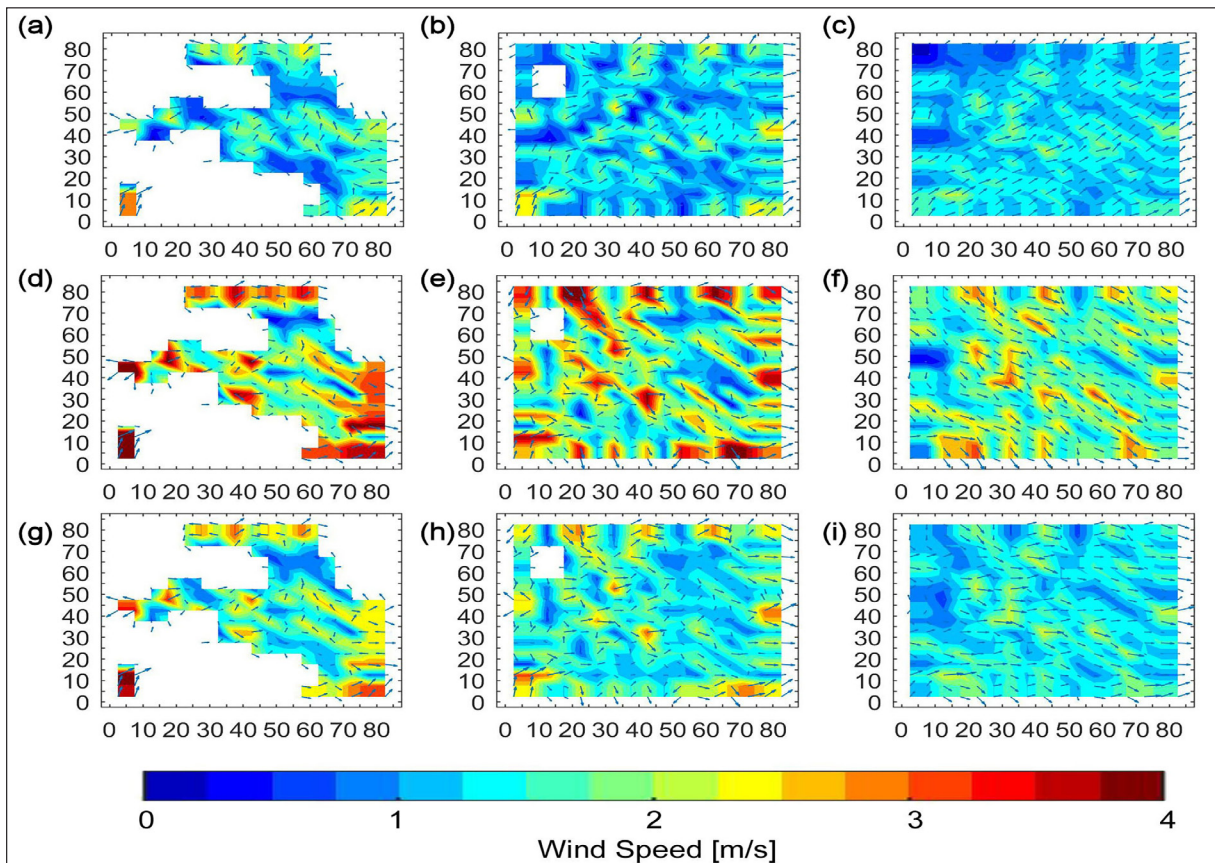


**Figure 3.** Wind fields simulation after 120 minutes for (a–c) January, (d–f) July, and (g–i) overall annual average. Each row subplots respectively show the simulation results for the model layer 8 (425–550 m asl), layer 10 (700–850 m asl), and layer 12 (1000–1150 m asl).

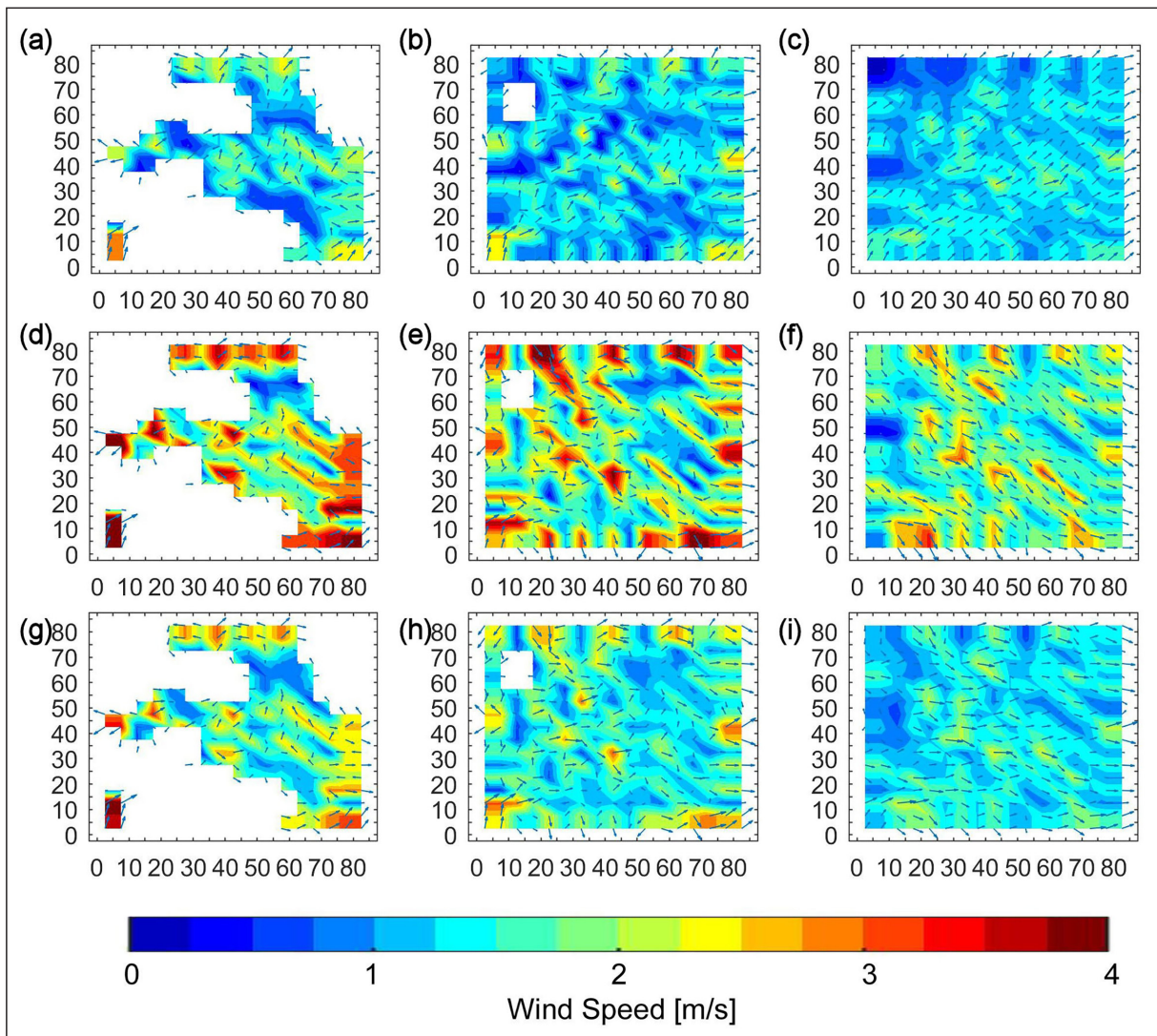


**Figure 4.** Wind fields simulation after 180 minutes for (a–c) January, (d–f) July, and (g–i) overall annual average. Each row subplots respectively show the simulation results for the model layer 8 (425–550 m.a.s.l.), layer 10 (700–850 m.a.s.l.), and layer 12 (1000–1150 m.a.s.l.).

As shown in Figure 5, the vertical component of wind velocity was the lowest (nearly zero in January and  $\sim 0.1$  m/s either up or down in July) near the surface. The vertical component increased (being slightly higher than 0.1 m/s in

January and higher than 0.2 m/s in July) due to turbulence with air parcels lifting up a layer-by-layer in the domain. The increasing rate of the vertical motion with a height was stronger in July than in January (Figure 5a–d).

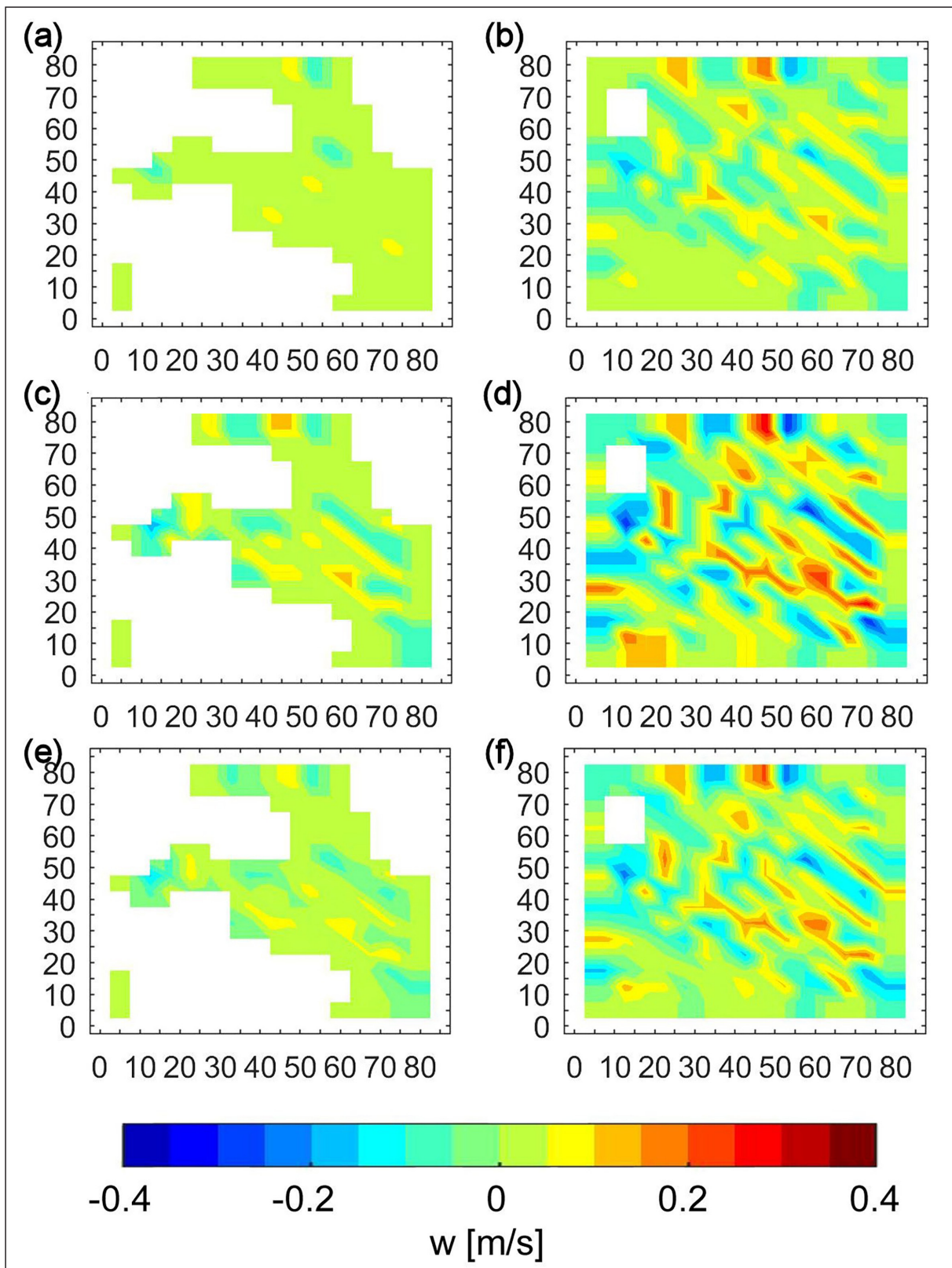


**Figure 5.** Vertical component of wind velocity simulated after 180 minutes for (a–b) January, (c–d) July, and (e–f) overall annual average. Each row subplots respectively show the simulation results for the model layer 8 (425–550 m.a.s.l.) and layer 10 (700–850 m.a.s.l.).

Conversely and as expected, the temperature differences between the surface and the atmosphere were higher near the surface than in the higher layers (Figure 6).

Furthermore, the temperature differences near the surface were higher in July than in January (reaching 1.5 °C versus 0.5 °C, respectively).

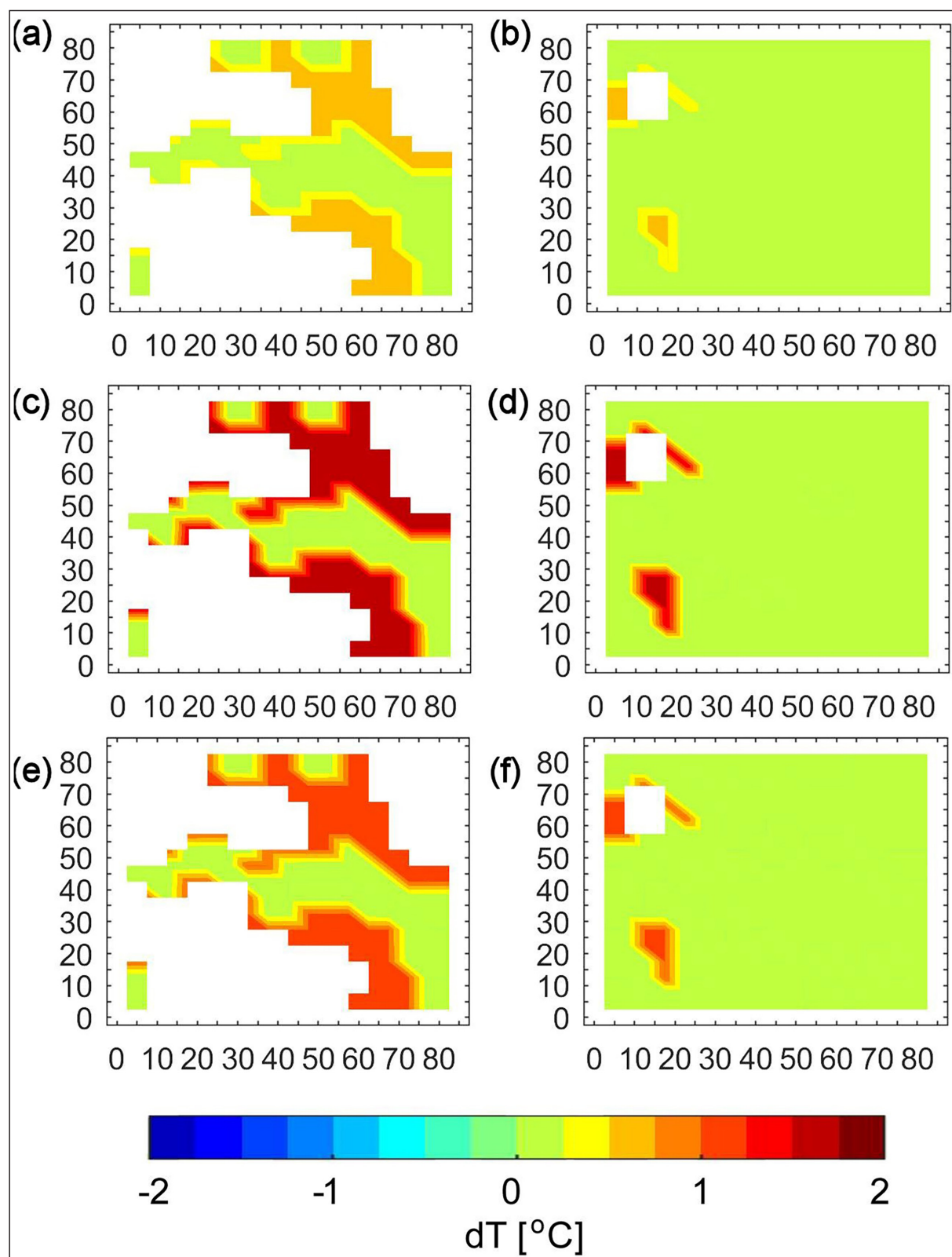


**Figure 6.** Temperature difference simulation after 180 minutes for (a–b) January, (c–d) July, and (e–f) overall annual average. Each row subplots respectively show the simulation results for the model layer 8 (425–550 m.a.s.l.) and layer 10 (700–850 m.a.s.l.).

#### 4. Summary and conclusions

In practice, nuclear safety is very strict, so that accidents are less probable to occur at a nuclear power plant (NPP). Nevertheless, accidents were reported several times over the past eighty years. Jordan is a developing country which relies on importing more than 90% of its energy needs. As a solution for the increasing energy demand in Jordan, the energy mix was planned to utilize nuclear power, and consequently, Jordan has started planning for the construction of NPPs. However, investigations of the meteorological conditions and mass transfer have never been conducted in relation to any of the suggested sites.

This study is aimed at stimulating and investigating the meteorological conditions (horizontal wind fields, vertical wind component, and surface temperature differences) near one of originally suggested geographical locations (the site of the Samra Energy Power Plant, SEPP) to construct a NPP in Jordan. The model domain had a size of 85×85 km<sup>2</sup> (17×17 horizontal grid points and 13 vertical layers) centering around the SEPP site (32.1443 °N, 36.1428 °E; 560 m a.s.l.), which is located in the northeastern part of Jordan. The model simulations were performed based on monthly-averaged meteorological conditions.

The model simulations revealed that the wind direction near the surface was developed to comply with the complexity of the terrain regardless of the input values of the prevailing wind direction. For instance, they propagated along the valleys surrounded by the dominating mountains. As for the wind speed near the surface, it was proportional to the input value of the wind speed; i.e. higher in summer than in winter. The wind speed was also proportional to the slope of the surrounding terrain. Quantitatively, the developed surface wind speed near the studied location was 1.3–2.0 m/s in January compared to 1.4–2.6 m/s in July. Along the valleys, the surface wind speed was 0.5–2.1 m/s in January compared with 1.0–4.3 m/s in July.

The vertical component of wind velocity was the lowest (negligible in January versus ~0.1 m/s in July) near the surface. As a result of the turbulence processes, the vertical wind speed increased (slightly higher than 0.1 m/s in January, while it was higher than 0.2 m/s in July).

It should be noted that this kind of investigation has never been conducted or reported before regarding the Jordanian conditions. The current study presented in this manuscript will hopefully serve as a base-block for other possible applications concerning other geographical locations in Jordan and also for assessment studies of the possible consequences in case of accidental releases from other potential objects with possible nuclear, chemical, and industrial danger.

#### Acknowledgment

Marwan Al-Kloub would like to thank colleagues from the University of Helsinki, Institute for Atmospheric and Earth System Research (UHES- INAR) for hosting him as a visiting researcher. He also would like to thank colleagues at INAR for useful discussions and constructive criticism. The Royal Jordanian Air Force and Prince Faisal Technical College are both acknowledged for supporting this work at the University of Jordan and for providing research mobility

for Al-Kloub. This work was scientifically supported by the Pan-Eurasian EXperiment (PEEX; <https://www.atm.helsinki.fi/peex>) Programme, the Academy of Finland Center of Excellence Programme (CoE-ATM, grant no. 307331). The INEP's Model Package (METEO and TRANS) was initially setup, tested, and optimized at the Center for Science Computing (CSC; [www.csc.fi](http://www.csc.fi)) HPC Sisu supercomputer.

#### References

AGROS, <https://pdc-argos.com/index.html>, accessed on June 19, 2019.

Baklanov, A. (2003). Evaluation of Dose, Risk, Vulnerabilities and Consequences for Population and Environment in Euro-Arctic Region. Danish Meteorological Institute, Sci. Rep. 03–18.

Baklanov, A., and Mahura, A. (2001). Atmospheric Transport Pathways, Vulnerability and Possible Accidental Consequences from Nuclear Risk Sites: Methodology for Probabilistic Atmospheric Studies. Danish Meteorological Institute, Sci. Rep. 01–09.

Baklanov, A., Mahura, A., Jaffe, D., Thaning, L., Bergman, R., Andres, R. (2002). Atmospheric Transport Patterns and Possible Consequences for the European North after a Nuclear Accident. *Environ. Radioac.* 60: 1–26.

Baklanov, A., Mahura, A., Morozov, S. (1994). The Simulation of Radioactive Pollution of the Environment after a Hypothetical Accident at the Kola Nuclear Power Plant. *Environ. Radioac.* 25: 65–84.

Baklanov, A., Mestayer, P., Clappier, A., Zilitinkevich, S., Joffre, S., Mahura, A., Nielsen, N. (2008a). Towards improving the simulation of meteorological field in urban areas through updated / advanced surface fluxes description. *Atmos. Chem. Phys.* 8: 523–543.

Baklanov, A., Morozov, S., Naumov, A., Amosov, P., Mahura, A., Fedorenko, Y., Rigina, O., Koshkin, V. (2000). Assessment of Potential Risk for Kola's Population from Radiological Impact of Accident on Spent Nuclear Fuel Facilities. Res. Rep., OCB-RW Project. 98: 03–26.

Baklanov, A., Sørensen, J., Mahura, A. (2008b). Methodology for Probabilistic Atmospheric Studies using Long-Term Dispersion Modelling. *Environ Model Assess.* 13: 541–552.

Cao, B., Zheng, J., Chen, Y. (2016). Radiation Dose Calculations for a Hypothetical Accident in Xianning Nuclear Power Plant. *Sci. Technol. Nucl.* ID 3105878.

Christoudias, T., Proestos, Y., Lelieveld, J. (2014). Atmospheric Dispersion of Radioactivity from Nuclear Power Plant Accidents: Global Assessment and Case Study for the Eastern Mediterranean and Middle East. *Energies* 12: 8338–8354.

Davydova, G.V., Morozov, S.V., Sharouuox G.A. (1990). The Methods of Mathematical Modelling of the Distribution of Radioactive Pollution from Nuclear Power Plants. Institute of Nuclear Energy of Academy of Science of Byelorussia, Minsk, p. 20, (in Russian).

Evangelidou, N., Hamburger, T., Talerko, N., Zibtsev, S., Bondar, Y., Stohl, A., Balkanski, Y. (2016). Reconstructing the Chernobyl Nuclear Power Plant (CNPP) Accident 30 years after. A unique database of air concentration and deposition measurements over Europe. *Environ. Pollut.* 216: 408–418.

Glyshenko, A. N. et al. (1981). About method choice of distribution of radioactive pollution from nuclear power plants into atmosphere. In the Nuclear Power Plants 4, Atomenergoizdat, Moscow, P. 60, (in Russian).

Hussein, T., Juwhari, H., Al Kuisi, M., Alkattan, H., Lahlouh, B., Al-Hunaiti, A. (2018). Accumulation and Corse

Modes Aerosols Concentrations and Carbonaceous Contents in the Urban Background Atmosphere in Amman – Jordan. Arab. J. Geosci 11, 617.

INES, International Nuclear and Radiological Event Scale, <https://www.iaea.org/topics/emergency-preparedness-and-response-epr/international-nuclear-radiological-event-scale-ines>, accessed on June 19, 2019.

Kawamura, H., Kobayashi, T., Furuno, A., Usui, N., Kamachi, M. (2014). Numerical simulation on the long-term variation of radioactive cesium concentration in the North Pacific due to the Fukushima disaster. J. Environ. Radioact. 136: 64–75.

Lauritzen, B., Baklanov, A., Mahura, A., Mikkelsen, T., Sørensen, J. (2007). Probabilistic risk assessment for long-range atmospheric transport of radionuclides. J. Environ. Radioact. 96: 110–115.

Mahura, A., Baklanov, A., Sorensen, J., Parker, F., Novikov, V., Brown, K., Compton, K. (2005). Assessment of potential atmospheric transport and deposition patterns Russian Pacific fleet operation. Environ. Monit. Assess. 101: 261–287.

Mahura, A., Jaffe, D., Andres, R., Merrill, J. (1999). Atmospheric transport pathways from the Bilibino nuclear power plant to Alaska. Atmos. Environ. 33: 5115–5122.

Matsuda, N., Mikami, S., Sato, T. (2017). Measurements of air dose rates in and around houses in the Fukushima Prefecture in Japan after the Fukushima accident. J. Environ. Radioact. 166: 427–435.

Mazur, A., Bartnicki, J., Zwodziak, J. (2014). Operational model for atmospheric and deposition of air pollution. Ecol Chem Eng S. 21: 385–400.

Mészáros, R., Leelőssy, A., Vincze, C., Szűcs, M., Kovács, T., Lagzi, I. (2012). Estimation of the dispersion of an accidental release of radionuclides and toxic materials based on weather type classification. Theor Appl Climatol. 107:375–387.

Mitrakos, D., Potiriadis, C., Housiadas, C. (2016). An approach for estimating the radiological significance of a hypothetical major nuclear accident over long distance transboundary scales. Nucl. Eng. Des. 300: 422–432.

Momoshima, N., and Bondietti, E. (1994). The Radial Distribution of <sup>90</sup>Sr and <sup>137</sup>Cs in Trees. J. Environ. Radioact. 22: 93–109.

Srinivas, C., and Venkatesan, R. (2005). A simulation study of dispersion of air borne radionuclides from a nuclear power plant under a hypothetical accidental scenario at a tropical coastal site. Atmos. Environ. 39: 1497–1511.

World Climate Guide, Climates for Travel, <https://www.climatestotravel.com/climate/jordan>, accessed in December 2018.